Nanotechnology Perceptions
ISSN 1660-6795
www.nano-ntp.com

SYNTHESIS AND STRUCTURAL CHARACTERIZATION OF NICKEL FERRITE NANOPARTICLES: EFFECT OF CALCINATION TEMPERATURE ON PARTICLE SIZE, STRAIN, AND DEFECT DENSITY

UPASANA SARMA[1*], DR. SANJIB KARMAKAR[2], DR. SUNANDAN BARUAH[3],NAIRIKA DEKA[4], KIBRIYA SIDDIQUE[5]

[1]DEPARTMENT OF INSTRUMENTATION AND USIC, GAUHATI UNIVERSITY, JALUKBARI, GUWAHATI, INDIA*
[2]DEPARTMENT OF INSTRUMENTATION AND USIC, GAUHATI UNIVERSITY, JALUKBARI, GUWAHATI, INDIA
[3]CENTRE OF EXCELLENCE IN NANOTECHNOLOGY (COEN) ASSAM DOWN TOWN UNIVERSITY, PANIKHAITI , GUWAHATI, INDIA
[4]CENTRE OF EXCELLENCE IN NANOTECHNOLOGY (COEN), ASSAM DOWN TOWN UNIVERSITY, PANIKHAITI, GUWAHATI, INDIA
[4]DEPARTMENT OF INSTRUMENTATION AND USIC, GAUHATI UNIVERSITY, JALUKBARI, GUWAHATI, INDIA

Nickel ferrite nanoparticles (NPs) (NiFe2O4) were synthesized using the co-precipitation method. The resulting nanomagnets (A1, A2 and A3) were characterized using various techniques. The size of the nanomagnetic particles was estimated to be 7nm for A1, 10 nm for A2 and 16 nm for A3 based on the transmission electron microscopy (TEM) image and X-ray diffraction analysis (XRD) pattern (using the Debye–Scherrer equation). The Full Width at Half Maximum intensity (FWHM) decreases with the increase in calcination temperatures, i.e. FWHM of A1 is greater than that of A2 and FWHM of A2 is greater than that of A3. Diffraction peaks broaden either because of inhomogeneous micro strain induced by dislocation-like defects (strain broadening) or because of shrinkage of coherent scattering volume (size broadening). The observed broadening of peaks is likely the combined result of both effects. Strain broadening and size broadening can be separated by WH plotting. Scanning electron microscopy (SEM) images of uncoated NiFe2O4 NPs is also done. NiFe2O4 NPs can be proposed as a viable material for biomedical applications.

Introduction

Nanostructured materials are being intensively studied as their physical properties vary from those of the bulk[1-2]. Ferrites are a group of technologically important magnetic materials of recent interest. Similar to transition metal oxides like MnO, FeO and CoO; the $NiFe_2O_4$ has

attracted much attention in recent years for its catalytic, electronic, dielectric and magnetic properties[3-9]. Cubic nanosized spinel ferrites bearing the formula MFe_2O_4 can be used for numerous applications, such as high-density information storage media, drug delivery, medical diagnostics, ferrofluid technology, electronic devices, catalysts, sensor technology and microwave applications [10-14].They possess unique magnetic, chemical and mechanical properties. It is well known that the properties of ferrite materials strongly depend on their preparation conditions. It is reported that Spinel $NiFe_2O_4$ nanocrystalline particles exhibit a mixed spinel structure with $Ni2^+$ ions occupying both tetrahedral and octahedral sites, but the bulk $NiFe_2O_4$ is a well- known inverse spinel, with $Ni2^+$ ions occupying only the octahedral sites[15]. Because of this structural changes, nanocrystalline $NiFe_2O_4$ is shown to exhibit interesting magnetic properties with respect to spin structure, curie temperature, coercivity etc.[16]. A variety of methods have been used to prepare nanosized ferrite particles. Among those methods, the sonochemical method is used for the preparation of $NiFe_2O_4$ nanoparticles. Classical Williamson–Hall (WH) method which is usually used for structural study is not suitable in case of elastically anisotropic materials because of strain anisotropy[17]. The effect of strain anisotropy is taken into account in X-ray diffraction by the dislocation contrast factors using modified Williamson–Hall (MWH) method[18-19] for structural study.

Study of growth of thin films of nickel ferrite nanoparticles prepared by Pulsed-laser deposition (PLD) is already carried out[20].

Here, we report the characterization of nickel ferrite nanocrystalline particles by X-ray diffraction, SEM with energy dispersive X-ray fluorescence spectrometer (EDX) and transmission electron microscopy (TEM). By measuring the relative peak shift in accordance with the material deformation at temperatures 773 K, 973 K and 1173 K, the lattice strain in individual phases is calculated, which can be further used to compute the phase-based temperature effect in the material. The radial peak broadening is also critically observed which can result from inhomogeneous strain (e.g. dislocations) and/or reduction of the coherent scattering size (e.g. substructure formation). Since lattice deformation induced peak broadening has multiple potential risks, therefore it is required to carry out careful analysis to extract useful quantitative information about the microstructure.

The present work aims to establish a comprehensive understanding of the behavior of the temperatures and structural properties in nickel ferrite nanoparticles. Importance is given to find out the effect of temperature on particle size, strain and type of defects in the $NiFe_2O_4$ nanocrystalline powder prepared at 773 K, 973 K and 1173 K. The type of dislocation and its density are calculated by the MWH method. The presence of dislocation is also confirmed by TEM analysis. The use of TEM for the study of defects in Sn-Doped GaAs Films Grown by Molecular Beam Epitaxy[21] and the studies of the Structure of Grain Boundaries in Al_2O_3 are already reported[22].

Materials and Methodology:

Materials: $FeCl_3$,$NiCl_3.6H_2O$ and NaOH

Synthesis of $NiFe_2O_4$ Nps:0.75 g; 9.3mmol, 50mL aqueous solution of $FeCl_3$ is mixed with 0.5g; 4.2mmol 50mL $NiCl_3.6H_2O$ in a bottom flask and placed in an ultrasonic bath (A). A 3 M 25 mL aqueous solution of NaOH is prepared. Both of these salt solutions are sonicated for 30 min to remove the dissolved oxygen. In a ultrasonic bath (JEIO Lab ompanion, Model:

1505) the aqueous solution of NaOH is added drop wise to the acidic solution of A under argon atmosphere with continuous ultrasonic irradiation operating at a frequency of 40KHz and a power of 40kW.After mixing, the pH of the salt solution is continuously maintained at 13-14. The temperature of the bath is raised upto 330K and is further sonicated for 30 min in air atmosphere. Formation of black precipitation is observed and subsequently separated by ultracentrifugation for 15 min. Black precipitation is washed with distilled water and ethanol.

Characterization techniques: The characterization of nickel ferrite nanocrystalline particles by X-ray diffraction, (UV-Vis) spectroscopy, SEM with energy dispersive X-ray fluorescence spectrometer (EDX) and transmission electron microscopy (TEM) are carried out.

Results and discussion

XRD analysis

The diffraction patterns of $NiFe_2O_4$ nanoparticles prepared at different calcination temperatures viz. 573K, 773K, 973K and 1173 K are recorded in a Philips X'pert Diffractometer which are marked as a, b, c and d respectively (Fig. 1).

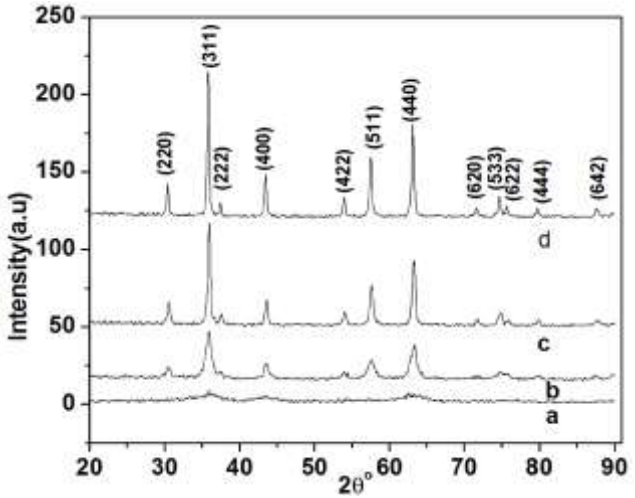

Fig.1 XRD spectra of $NiFe_2O_4$ nanoparticle prepared at calcinations temperature (a) 573K (b)773K and (c) 973K (d) 1173K.

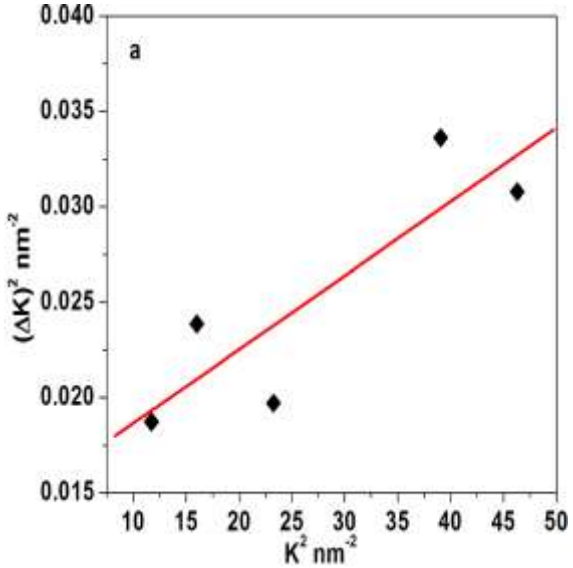

Fig.2 WH plot of (a) A1, (b) A2 and (c) A3.

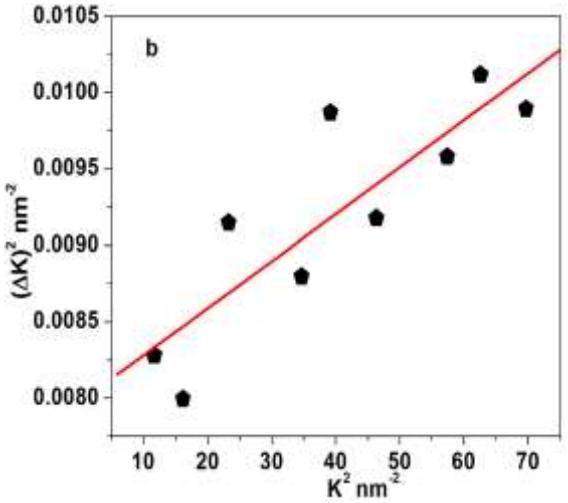

Fig.2(b) WH plot of A2

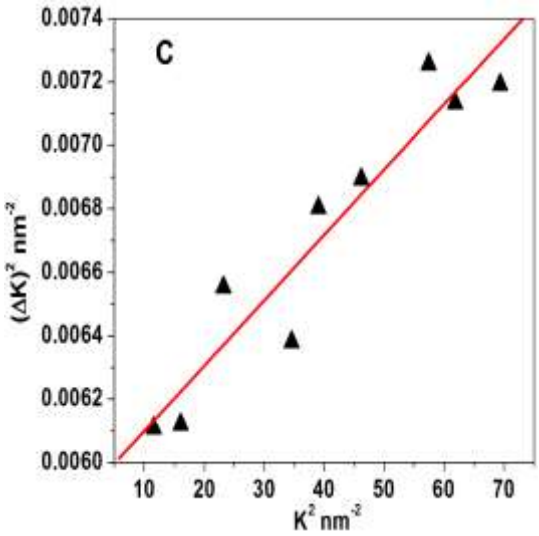

Fig.2(c) WH plot of A3

The diffractometer is calibrated with a standard silicon sample and the data are collected at 40 kV, 30 mA, 0.5 s/step and the step size is 0.02º. The particle size and strain of the nanoparticles prepared at 773 K (A1), 973 K (A2) and 1173 K (A3) are measured by classical WH method. The prepared nanoparticles at room temperature show amorphous nature and the diffraction pattern of that is not shown. The peaks of A1, A2 and A3 are fairly close to that of standard nickel ferrite (SNF) samples (ICDD card no. 86-2267). The SNF is a cubic structure with lattice constant a=b=c=8.337 (4) Å and belongs to the space group Fd(-3)m (227). The d-values of A1, A2 and A3 are calculated with the peaks obtained from the XRD pattern using Bragg's law which are fairly close to that of the SNF. This also suggests that the $NiFe_2O_4$ nanoparticles are successfully prepared at temperatures 773 K, 973 K and 1173 K. The anisotropy of the width of the peaks is observed in all samples prepared at temperatures 773 K, 973 K and 1173 K. The observed anisotropy of the width of the peaks is due to the fact that when the particle sizes of the nanoparticles are decreased, the intensities of the diffraction peaks are decreased and the corresponding widths of the peaks are increased. As the sizes of the nanoparticles are not equal in all directions, the widths of the peaks are different in different directions of diffraction maxima. The observed shifts in the peaks of the nanoparticles are because of the development of defects in the nanoparticles at higher calcination temperatures. During deformation, the d-spacing for a given (hkl) plane will change (i.e. peak shift) and the associated lattice strain are calculated by the equation (3)

As A1, A2 and A3 are also fall in cubic system, the calculated lattice parameters are found to be 8.313 (4) Å, 8.324 (3)Å and 8.332 (5) Å for A1, A2 and A3 respectively, which are determined by the following equation,

$$a = d(h^2 + k^2 + l^2)^{1/2} \quad (1)$$

where'd' is the perpendicular distance between the two consecutive atomic planes in the lattice and the (hkl) are the Miller indices. The lattice constants are calculated from the peaks of high intensities.

The lattice parameters of the $NiFe_2O_4$ nanoparticles are linearly dependent on the calcination temperature. As shown in Fig.1, the peaks of A1, A2 and A3 are much stronger than that of $NiFe_2O_4$ nanoparticles prepared at 573 K. At lower temperature the diffraction peaks of the nanoparticles are broadened. This shows that the degree of crystallinity of $NiFe_2O_4$ nanoparticles increases at higher calcination temperatures with increase in particle sizes.

During the increase in calcination temperature, not only the peak centers but also the peak widths gradually changed with strain. The Full Width at Half Maximum intensity (FWHM) is also decreased with the increase in calcination temperatures, i.e. FWHM of A1 is greater than that of A2 and FWHM of A2 is greater than that of A3. Diffraction peaks broaden either because of inhomogeneous micro strain induced by dislocation-like defects (strain broadening) or because of shrinkage of coherent scattering volume (size broadening). The observed broadening of peaks is likely the combined result of both effects. Strain broadening and size broadening can be separated by WH plotting.

To calculate the particle size and strain, the instrumental broadening of each reflection is corrected using the following equation[23]

$$\Delta\theta = B(1 - \frac{b^2}{B^2})^{1/2} \quad (2)$$

where B is the FWHM of the analyzed diffraction line and b is the FWHM of the diffraction line of Si reference powder.

We have used in our study the classical Williamson and Hall method for the calculation of lattice strain and particles size simultaneously using the following relation,

$$(\Delta K)^2 = 4e^2K^2 + (\frac{0.9}{D_{WH}})^2 \quad (3)$$

where $\Delta K = 2\Delta\theta\cos\theta/\lambda$, $\Delta\theta$ =FWHM, D_{WH} = average particle size, $K=2\sin\theta/\lambda$, 2θ = Braggs angle in degrees, λ= Wavelength of CuK_α radiations (1.5406Å) and e= lattice strain.

A graph is plotted K^2 vs. $(\Delta K)^2$ taking the values of 2θ and FWHM of only (220), (311), (400), (511) and (440) prominent peaks for samples A1, A2 and A3 (Fig.2). The classical WH plots show a strain anisotropy is present in all samples (A1, A2 and A3).The average particle size of $NiFe_2O_4$ nanoparticles prepared at 773 K (A1) is less than that of $NiFe_2O_4$ nanoparticles prepared at 973 K (A2) and 1173 K (A3).

The average particle size of A1, A2 and A3 are found to be of the order of (7±1.8234) nm, (10 ± 0.3871) nm and (12 ± 0.2337) nm respectively. This confirms that the size of the particles increases with the increase in calcination temperature. The lattice strain of A1, A2 and A3 are calculated from the slope of the classical WH plot (Fig. 2) and are found to be of the order of (9.8380± 1.6106) $x10^{-3}$, (2.7730 ± 0.3120)$x10^{-3}$and (2.2675± 0.0120)$x10^{-3}$ respectively.

The effect of strain anisotropy is taken into account in X-ray diffraction by the dislocation contrast factors using modified Williamson–Hall (MWH) method for determination of dislocation and is density by the following equation[24-27]

$$(\Delta K)^2 = (\frac{\pi b^2 \rho}{2B})K^2 C_{hkl} + (\frac{0.9}{D_{MWH}})^2 \quad (4)$$

where, D_{MWH} is average crystallite size, 'ρ' is the average dislocation density, b is the modulus of Burgers vector of dislocation (for f.c.c. crystals, **b**=(a/2)$^{1/2}$, where 'a' lattice parameter), C_{hkl} is the dislocation contrast factor for the (hkl) reflection and B is a constant that can be taken as 10 for a wide range of dislocation distribution. For a cubic crystal, the contrast factor C_{hkl} is related to the contrast factor of Bragg reflection (h00) as given by the equation[24]

$$C_{hkl} = C_{h00}(1 - qH^2) \quad (5)$$

where, $H^2=(h^2k^2+k^2l^2+l^2h^2)/(h^2+k^2+l^2)^2$ for cubic crystals and 'q' is a parameter which depends on the elastic constants and type of dislocation. The 'C_{h00}' and 'q' values for screw and edge dislocations can be obtained using the relations [25, 28]

$$C_{h00} = a(1 - e^{\frac{-A_i}{b}}) + cA_i + d \quad (6)$$

$$q = a_1(1 - e^{\frac{-A_i}{b_1}}) + c_1A_i + d_1 \quad (7)$$

where, A_i is the elastic anisotropy constant which can be given as

$$A_i = 2\frac{C_{44}}{C_{11}-C_{12}} \quad (8)$$

where C_{11}, C_{12} and C_{44} are elastic constants; a, b, c and d in Eq. (6) and a_1, b_1, c_1 and d_1 in Eq. (7) are parameters which depend on the type of dislocations and may depend on the elastic constant ratio C_{12}/C_{44}.The reported values of elastic constants C_{11}, C_{12} and C_{44} for $NiFe_2O_4$ are 273.1, 160.7 and 82.3 GPa respectively[29]. Though the above values of elastic constants are of bulk single crystals, these values can also be used for calculation of elastic anisotropic constant A_i for nanoparticles. A similar type of work for determination of strain due to defects and its density for chemically prepared PbS nanoparticles are reported[30]. The value of A_i is calculated from Eq. (8) using the reported values of C_{11}, C_{12} and C_{44} for $NiFe_2O_4$ and is found to be 1.464. Similarly, the value of C_{12}/C_{44} ratio for $NiFe_2O_4$ is also calculated from the reported values of C_{12} and C_{44} which is found to be 1.952.The values of constants a=0.1740, b=1.9522, c=0.0293, d=0.0662; and a_1=5.4252, b_1=0.7196, c_1=0.0690, d_1= -3.1970 are same for all materials of f.c.c structure in which screw dislocation is present and is independent of C_{12}/C_{44}[19] Using the value of elastic anisotropy constant A_i (1.464) and the above mentioned values of constants of f.c.c. structure the value of 'C_{h00}'and 'q' are calculated from Eq. (6) and (7) which are found to be of the order of 0.2009 and 1.6202 respectively for screw type of defect . For edge dislocation in f.c.c. crystals, the values of a, b, c, d and a_1, b_1, c_1, d_1 depend on C_{12}/C_{44} and which are reported for the values of C_{12}/C_{44}. As the value of C_{12}/C_{44} for $NiFe_2O_4$is 1.952, the required value of 'a' is determined from the graph corresponding to C_{12}/C_{44} = 1.952 which is found to be 0.02640. Similarly, the values of other parameters are determined which are found to be of the order of b=1.9345, c=0.0192, d=0.0698, a_1=6.3445, b_1= 0.7624, c_1=0.8299, and d_1= -4.8877.Using the above mentioned values of constants, the values of 'C_{h00}'and 'q' are calculated from Eq. (6) and (7) which are found to be of the order of 0.2166 and 0.6964 respectively for edge type of defect. Now using the values of 'C_{h00}'and 'q' for screw and edge defects, the different values of dislocation contrast factors $C_{hkl}$of $NiFe_2O_4$ are calculated and given in Table 1.

Now a MWH graph, ΔK^2 vs K^2C_{hkl} is plotted for $NiFe_2O_4$ nanoparticles prepared at 773K, 973 K, 1173K at different proportions of screw and edge.

It is found that for the samples A1, A2 and A3, the best fitting of MWH curves are obtained at proportion (10%S , 90% E) ; (100%S , 0%E) and (10%S, 90%E) of screw and edge dislocations respectively. The defect density for the sample prepared at calcination temperatures 773 K, 973 K and 1173 K corresponding to the above mentioned proportions are found to be $(2.283 \pm 0.7546) \times 10^{16}$ m^{-2} $(6.6149 \pm 0.8614) \times 10^{15}$ m^{-2} and (4.1602 ± 0.3123) x

10^{15} m^{-2} respectively. Particle sizes calculated from MWH plot corresponding to the calcination temperatures 773 K, 973 K, and 1173 K are found to be of the order of(7± 1.9201) nm, (10 ± 0.3262) nm and (12 ± 0.1536) nm respectively. The values of particle size calculated by the MWH method are more accurate than that of the WH method. MWH curve for sample A3 at different proportions of screw and edge is shown in Fig.3.

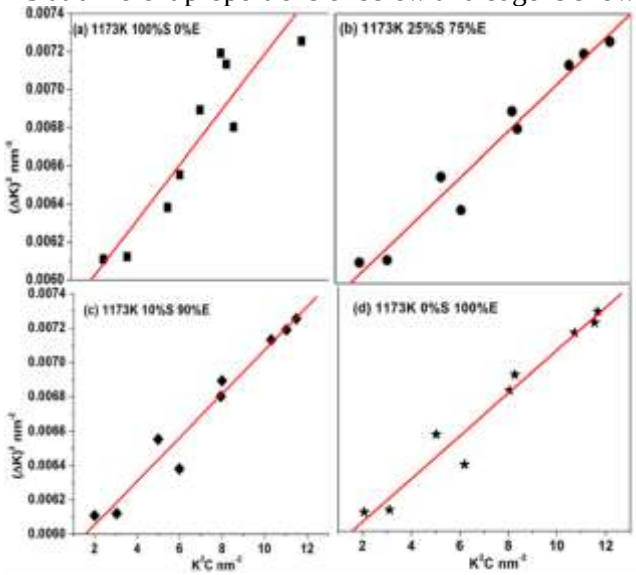

Fig.3. MWH plot for A3 at different proportion of screw and edge defects: (a)100%S 0%E ,(b) 90%S 10%E, (c) 75%S 25%E, (d) 50%S 50%E.

TEM analysis:

The HRTEM (TEM, Jeol JEM 2100 200 K_v) images of one of the samples A3 are shown in Fig. 4. The selected area diffraction pattern (SAED) is also shown in inset of Fig.4b. It is clearly seen that the sample contains spherical as well rectangular particles. The average particle size is found to be of the order of 7nm for A1, 10 nm for A2 and 16 nm for A3. These values are almost matched with the average particle sizes obtained from XRD results. As the lattice planes are clearly visible in Fig.4b, the well crystallinity of the prepared nanoparticles is confirmed. Two lattice planes with index (311) and (440) are marked in the Fig.4b of the HRTEM image, In the TEM micrograph, the presence of screw and edge dislocations of one nanoparticle (A3)are observed and marked by red circles (Fig4b). However, to observe closely the presence of screw dislocation, a 3D image of lattice planes may be required.

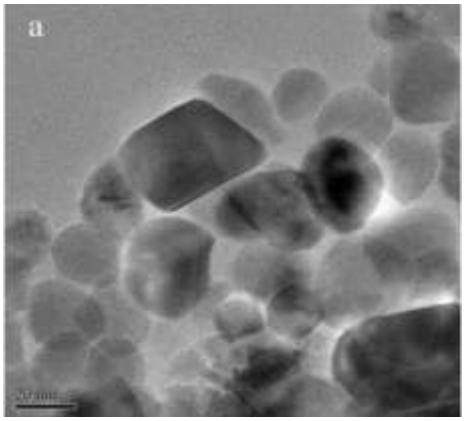

Fig.4a HRTEM image of A3.

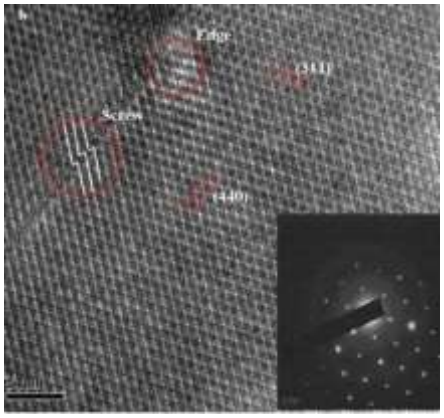

Fig.4b. Magnified view of lattice spacing where screw and edge dislocations are marked by red circles, (311) and (440) lattice planes are shown. SAED image is shown in the inset.

SEM analysis

The SEM (Ziezz sigma VP advance) image of $NiFe_2O_4$ nanoparticles prepared at different calcination temperatures of 773K, 973K and 1173 K show the non uniformity of the surface of prepared nanoparticles. The SEM image of A3 is shown in Fig.5.

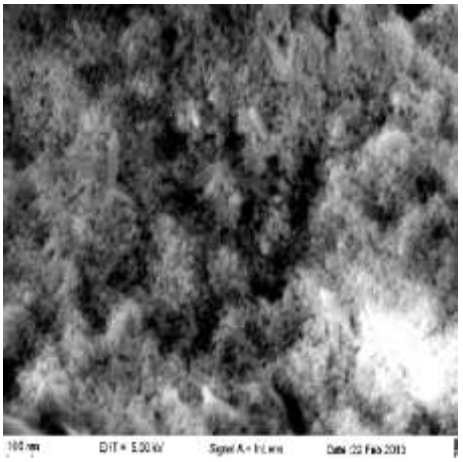

Fig.5. SEM image for surface morphology of A3

From the EDX spectra, the ratio of Ni:Fe is found to be of 1:2 (Table 1))which confirms that prepared $NiFe_2O_4$ nanoparticles are stoichiometric. The presence of carbon in the EDX result is due to the carbon coating of the sample during data collection.

Table. 1. Average dislocation contrast factors, density of Bragg reflections of $NiFe_2O_4$

Dislocation contrast factor	**Sample A1**	**Sample A2**	**Sample A3**
C_{220}	0.1126	0.1195	0.1729
C_{311}	0.1415	0.1417	0.1886
C_{400}	0.1905	0.2009	0.215
C_{422}	---------	0.1195	0.1729
C_{511}	0.1687	0.1761	0.2032
C_{440}	0.1126	0.1195	0.1729
C_{620}	---------	0.1716	0.1998
C_{533}	---------	0.1074	0.1666
C_{444}	---------	0.0923	0.1589

Dislocation density m^{-2} $(2.2830 \pm 0.7546) \times 10^{16}$ $(6.6149 \pm 0.8228) \times 10^{15}$ $(4.1602 \pm 0.0032) \times 10^{15}$

Table.2. Elements present in $NiFe_2O_4$ nanoparticles with weight and atomic percentage.

Element	**Weight**	**Atomic %**
C	23.58	38.42
O	40.12	49.07
Fe	23.95	8.39
Total	100	

Conclusion

$NiFe_2O_4$ nanoparticles are successfully prepared at calcination temperatures 773 K, 973 K and 1173 K. The structural properties of $NiFe_2O_4$ nanoparticles at different calcination temperatures are presented. X-ray diffraction patterns and SEAD image of HRTEM show well crystallinity of the prepared nanoparticles. The stoichiometry of the $NiFe_2O_4$ nanoparticles is confirmed by EDX results. X-Ray diffraction line profile analysis using WH and MWH methods are carried out to determine the particles size, microstrain, dislocation and its density. The particle sizes obtained from XRD and TEM are compared which are found to be almost equal and increased with the increase in calcination temperatures. As the particle size is increased, the corresponding strain associated with the nanoparticles decreases. Since the formation of lattice defects is a random phenomenon, it has no linear variation with the temperature of the nanoparticles at which it is prepared. But the presence of strain anisotropy seen in the WH curve in all samples can be resolved by MWH method by considering various proportions of screws and edges. Therefore, the MWH method gives more corrected values of particle size and strain. The screw and edge dislocations mainly induce the strain of the nanoparticles prepared at 773 K and 1173 K but the strain of the nanoparticles prepared at 993 K is induced by screw only.

Acknowledgment

We thank SAIF, Department of Instrumentation & USIC, Gauhati University, COEN (Assam Down town University) Guwahati-781014, SAIF, NEHU, Shillong and the Institute of Advanced Study in Science & Technology (IASST), Guwahati, India for providing XRD, TEM and SEM facilities.

Reference

1. Ozin, GA. (1992) .AdV. Mater.4, 612. DOI: 10.1002/adma.19920041003
2. Gleiter H. (1992).AdV. Mater.4, 474. DOI: 10.1002/adma.19920040704
3. Che,Y.K. Datar, A. Yang, X. M.Naddo, T. Zhao, J.C.&Zang, L. (2007). J. Am. Chem. Soc. 29, 6354– 6355.
4. Ahmad, M.M.Makhlouf, S.A.&Khalil, K.M.S. (2006).J. Appl. Phys. 100, 094323.
5. Schmidt-Mende, L. & MacManus-Driscoll, J.L. (2007).Mater. Today 10,40–48.
6. Wan, Q.Dattoli, E.N. & Lu, W. (2007).ApplPhysLett 2007;90 :222107
7. Shrestha, S.Yeung, C.M.Y. Nunnerley, C. Tsang, S.C. & Sens. (2007). Actuators A.136, 191–
8. 198.
9. Subramania, A.Saradha, T.&Muzhumathi, S. (2007). J. Power Sources. 167, 319–324.
10. Hara, S.&Miyayama, M. (2004). Solid State Ionics.168, 111–116.
11. Kodama, RH. (2000) J.Magn.Magn.Mater.200, 359-372.

12. Kavas, H. Baykal, A. Toprak, M.S. Koseoglu, Y. Sertkol, M. &Aktas, B. (2009). J. Alloys Compd. 479, 49-55
13. dePaiva, J.A.C.Graça, M.P.F.Monteiro, J.Macedo, M.A.& Valente, M.A.(2009). J. Alloys Compd. 485, 637-641
14. Alarifi.A, Deraz, N.M.&Shaban, S. (2009).J. Alloys Compd. 486, 501-506.
15. Farea, A.M.M. Kumara, S. Batoo, K.M. & Lee, A.Y.C.G. (2009). J Alloys Compd. 469, 451-457.
16. Chinnasamy, C.N.Narayanasamy, A.Ponpandian, N.Chattopadhyay, K.Shinoda, K.Jeyadevan, B.Tohji, K. Nakatsuka, K.Furubayashi, T. & Nakatani, I. (2001).Phy.Rev. B.63,184108.
17. Kodama, R.H.& Berkowitz, A.E.(1999).Phys. Rev. B. 59, 6321.
18. Williamson, G.K& Hall, W.H. (1953).Acta Metall 1, 22–31.
19. Shen, T.D. Schwarz, R.B. & Thompson, J.D.(2005). Phys. Rev. B. 72, 014431-1-8.
20. Ungar, T. & Tichy, G.(1999). Phys. Status.Solid. A. 171,425–34.
21. Johnson, M.T.Kotula, P.G.&Carter, C.B. (1999).Journal of Crystal Growth. 206, 299-307.
22. Chen, S.H. Carter, C.B. & Enquist, P. (1987). Appl. Phys. A. 44, 143-151.
23. Carter, C.B.Kohlstedt, D.L.&Sass, S.L. (1980). J. Am. Ceram.Soc. 63, (11-12) 623-627.
24. Klug, H.P.& Alexander, L.E.(1974). X-ray Diffraction Procedures for Polycrystalline and
25. Amorphous Materials, Second ed. New York : John Wiley & Sons.
26. Ungar, T.Dragomir, I.Revesz, A.& Borbely, A. (1999). J. Appl.Crystallogr.32,992–1002.
27. Ungar, T. &Tichy, G.(1999). Phys. Status.Solid. A. 171,425–34.
28. Revesz, A.Ungar, T.Borbely, A. & Lendvai, J. (1996).Nanostruct Mater 7,779–88.